J Nanostruct 16(4): 5131-5149, Autumn 2026

RESEARCH PAPER

Soluplus-Stabilized Atorvastatin Calcium-Loaded Spanlastic Nanovesicles: Formulation Optimization, In Vitro Characterization, and Ex Vivo Intestinal Permeation

Marwa Majid Mohammed Salih [1,2] *, *Ahmed A. A. Alsaad* [1]

[1] *Department of Pharmaceutics, College of Pharmacy, University of Basrah, Iraq*

[2] *Ministry of Health, Maysan Health Directorate, Maysan, Iraq*

ARTICLE INFO

Article History:
Received 17 May 2026
Accepted 22 August 2026
Published 01 October 2026

Keywords:
Box–Behnken design
Drug release
Intestinal permeation
Soluplus
Spanlastic nanovesicles

ABSTRACT

Poor aqueous solubility can limit the dissolution and oral performance of Biopharmaceutics Classification System (BCS) class II drugs, including atorvastatin calcium (ATC). This study developed Soluplus-stabilized ATC-loaded spanlastic nanovesicles (ATC-SNVs) by ethanol injection and optimized them using a three-factor, three-level Box-Behnken design. Particle size, polydispersity index (PDI), and entrapment efficiency (EE%) were evaluated as formulation responses. The selected formulation was further characterized for zeta potential, deformability, morphology, differential scanning calorimetry (DSC), apparent solubility, apparent in vitro drug release, and ex vivo intestinal permeation. The selected formulation, containing a Span 60:Tween 80 ratio of 7:3, Soluplus 25 mg, and a sonication time of 10 min, showed a particle size of 59.63 nm, PDI of 0.277, zeta potential of –43.1 mV, and EE of 84.0%. DSC findings indicated reduced detectable ATC crystallinity but did not independently confirm chemical compatibility or molecular incorporation. Compared with pure ATC dispersion, ATC-SNVs exhibited higher apparent solubility and greater apparent in vitro drug transfer across the dialysis membrane, with approximately two-fold increases in ex vivo flux and apparent permeability coefficient (Papp). These findings indicate that Soluplus-stabilized spanlastic nanovesicles may improve the pharmaceutical performance and intestinal permeation of ATC. However, independent optimization confirmation, long-term stability studies, and in vivo pharmacokinetic evaluation are required before improved oral bioavailability can be established.

How to cite this article
Mohammed salih M., Alsaad A. Soluplus-Stabilized Atorvastatin Calcium-Loaded Spanlastic Nanovesicles: Formulation Optimization, In Vitro Characterization, and Ex Vivo Intestinal Permeation. J Nanostruct, 2026; 16(4):5131-5149. DOI:10.22052/JNS.2026.04.053

INTRODUCTION

Poor aqueous solubility remains a major formulation challenge: approximately 40% of approved drugs and nearly 90% of drug candidates have been reported to be poorly water-soluble [1]. According to the Biopharmaceutics Classification System (BCS), class II compounds are characterized by low solubility and high permeability; for such compounds, dissolution commonly represents the rate-limiting step for oral absorption [2,3].

* *Corresponding Author Email: marwaa.majid@uobasrah.edu.iq*

Consequently, formulation strategies that increase apparent solubility, dissolution rate, or the concentration of dissolved drug available for absorption are particularly relevant to BCS class II drug development [1,4].

Nanoparticulate and vesicular drug-delivery systems have been investigated as approaches to improve the pharmaceutical performance of poorly water-soluble drugs [4]. Spanlastics are elastic, surfactant-based nanovesicles composed of a non-ionic surfactant and an edge activator. Kakkar and Kaur introduced spanlastics as a nanovesicular platform in 2011 and demonstrated that inclusion of an edge activator can increase vesicle elasticity and membrane permeation [5]. Subsequent work has extended spanlastic systems to oral delivery and ex vivo intestinal permeation studies [6].

Soluplus is an amphiphilic graft copolymer used as a solubilizing and stabilizing excipient in several advanced drug-delivery systems [7]. A recent study by Alkufi and Kassab specifically evaluated Soluplus-stabilized nimodipine spanlastics and reported effects of the stabilizer on particle size, dispersity, deformability, and short-term formulation stability [8]. The use of Soluplus in atorvastatin calcium-loaded spanlastics remains insufficiently characterized; therefore, combining Soluplus with a deformable spanlastic carrier provides a rational formulation approach for improving ATC solubilization and intestinal transport.

Atorvastatin is a selective, competitive inhibitor of 3-hydroxy-3-methylglutaryl-coenzyme A (HMG-CoA) reductase, the rate-limiting enzyme in the conversion of HMG-CoA to mevalonate. Inhibition of this pathway reduces hepatic cholesterol synthesis and promotes increased hepatic LDL-receptor activity, thereby lowering circulating LDL cholesterol [9,10]. The position of HMG-

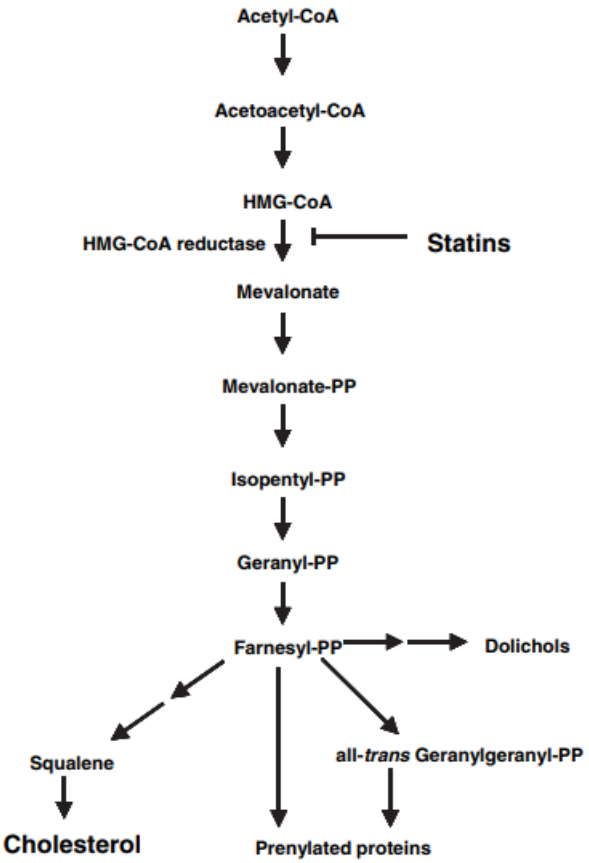

Fig. 1. Mammalian mevalonate pathway showing inhibition of HMG-CoA reductase by statins; PP, pyrophosphate. Adapted from Corsini et al. [9].

CoA reductase inhibition within the mevalonate pathway is illustrated in Fig. 1.

Atorvastatin is used to reduce elevated LDL-C, total cholesterol, apolipoprotein B, and triglycerides in several dyslipidemic conditions, with the exact indication and dose determined by the approved product labeling and patient characteristics [10].

Following oral administration, atorvastatin is rapidly absorbed, with maximum plasma concentrations generally occurring within 1-2 h. Its absolute bioavailability is approximately 14%, reflecting substantial presystemic clearance. Atorvastatin is highly protein bound, has a large apparent volume of distribution, is metabolized predominantly by CYP3A4 to active ortho- and para-hydroxylated metabolites, and has a plasma elimination half-life of approximately 14 h [10]. These pharmacokinetic characteristics, together with its low aqueous solubility, motivate formulation approaches intended to improve dissolution and intestinal presentation of the drug without assuming that ex vivo improvements will necessarily translate into higher systemic bioavailability.

The aim of this study was to formulate and optimize Soluplus-stabilized atorvastatin calcium-loaded spanlastic nanovesicles using a Box-Behnken design and to evaluate their physicochemical characteristics, apparent solubility, apparent in vitro release behavior, and ex vivo intestinal permeation. Specifically, the effects of the Span 60:Tween 80 ratio, Soluplus amount, and sonication time on particle size, PDI, and entrapment efficiency were investigated. Because no in vivo pharmacokinetic study was performed, the study was designed to assess formulation performance and intestinal permeation rather than to demonstrate increased oral bioavailability.

MATERIALS AND METHODS

Materials

Atorvastatin calcium was procured from Hetero Labs Ltd. (India). Soluplus was purchased from BASF SE (Germany). Span® 60 and Tween® 80 were procured from Hangzhou Hyper Chemicals Limited (China). All other chemicals and solvents were of analytical grade.

Box–Behnken Experimental Design

A three-factor, three-level Box-Behnken design (BBD) was employed to evaluate and optimize atorvastatin calcium-loaded spanlastic nanovesicles (ATC-SNVs). The design was generated and analyzed using Design-Expert® software (Version 13, Stat-Ease Inc., Minneapolis, MN, USA).

The investigated independent variables were the Span 60:Tween 80 ratio (A), Soluplus amount (B), and sonication time (C). Factor A was coded as 5:5 at the low level (-1), 7:3 at the center level (0), and 9:1 at the high level (+1), consistent with the coded regression equation and response-surface plots. Soluplus was evaluated at 0, 12.5,

Table 1. Independent formulation/process variables and coded levels used in the Box-Behnken design.

Factor	Code	Low (-1)	Center (0)	High (+1)
Span 60:Tween 80 ratio	A	5:5	7:3	9:1
Soluplus (mg)	B	0	12.5	25
Sonication time (min)	C	0	5	10

Table 2. Dependent responses and optimization goals used in the Box-Behnken design.

Response	Code	Goal
Particle size (nm)	Y1	Minimize
Polydispersity index	Y2	Minimize
Entrapment efficiency (%)	Y3	Maximize

and 25 mg, and sonication time at 0, 5, and 10 min. Factor levels are presented in Table 1. All other formulation and processing parameters were intended to be held constant throughout the design.

Particle size (PS; Y1), polydispersity index (PDI; Y2), and entrapment efficiency (EE%; Y3) were evaluated as responses, with the optimization goals summarized in Table 2. A total of 15 experimental runs, including three center-point replicates, were generated. Analysis of variance (ANOVA) was applied at $p < 0.05$. Model assessment included F-values, p-values, R^2, adjusted R^2, predicted R^2, adequate precision, and lack-of-fit statistics. Response-surface and diagnostic plots were used to examine model behavior within the investigated design space.

Preparation of ATC-Loaded Spanlastic Nanovesicles

ATC-loaded spanlastic nanovesicles (ATC-SNVs) were prepared by the ethanol-injection approach used for spanlastic formulations [5,6,8]. Atorvastatin calcium (5 mg) and Span 60 were dissolved in ethanol to form the organic phase. Tween 80 and Soluplus were dispersed/dissolved in distilled water to form the aqueous phase, which was maintained at 40-50 °C under magnetic stirring. The Span 60:Tween 80 ratio, Soluplus amount, and sonication time were varied according to the Box-Behnken design. The organic phase was added dropwise to the aqueous phase under stirring at 1000 rpm, followed by 60 min of stirring to facilitate solvent removal and vesicle formation. The dispersion was then sonicated for the time specified by the design and stored at 4 °C until characterization.

Characterization of ATC-Loaded Spanlastic Nanovesicles

Particle Size and Polydispersity Index Measurements

Particle size (z-average) and PDI were measured by dynamic light scattering using a Zetasizer Nano ZSP (Malvern Panalytical Ltd., Malvern, UK) after appropriate dilution with distilled water. Measurements were performed at 25 °C.

Determination of Entrapment Efficiency (EE%)

Entrapment efficiency (EE%) was determined using Amicon® Ultra centrifugal filter units (MWCO 10 kDa). Four milliliters of dispersion were transferred to the ultrafiltration device and centrifuged at 15,000 rpm for 30 min. The filtrate containing unentrapped ATC was collected, diluted with methanol, and analyzed by UV-visible spectrophotometry at 249 nm using a calibration curve prepared in methanol. EE% was calculated using Eq. 1.

$$EE\ (\%) = [(\text{Total ATC} - \text{Free ATC}) / \text{Total ATC}] \times 100$$

Characterization of the Selected ATC-Loaded Spanlastic Nanovesicles

The selected ATC-SNV formulation was further characterized by zeta potential, deformability index (DI), transmission electron microscopy (TEM), scanning electron microscopy (SEM), differential scanning calorimetry (DSC), apparent solubility, apparent in vitro release, and ex vivo intestinal permeation.

Zeta Potential Measurements

The zeta potential of the selected ATC-SNV formulation was measured using the Zetasizer Nano ZSP after appropriate dilution with distilled water. Measurements were performed in triplicate at 25 ± 0.5 °C and are reported as mean ± SD.

Deformability Index (DI)

Vesicle deformability was assessed by extrusion through a nylon membrane with a nominal pore size of 200 nm under a constant pressure of 1 bar. The deformability index was calculated as $DI = J (rv/rp)^2$, where J is the extrusion amount/flux term used in the calculation, rv is the vesicle size after extrusion, and rp is the membrane pore-size term [5,11].

Transmission Electron Microscopy (TEM)

For TEM examination, a drop of the diluted selected formulation was placed on a carbon-coated copper grid, negatively stained, air-dried, and examined by transmission electron microscopy.

Scanning Electron Microscopy (SEM)

For SEM examination, the lyophilized selected formulation was mounted on aluminum stubs, sputter-coated with gold, and imaged at suitable magnifications to characterize the morphology of the dried powder.

Differential Scanning Calorimetry (DSC)

DSC was used to compare the thermal behavior

of pure ATC, the physical mixture, and the selected ATC-SNV formulation. Approximately 5 mg of each sample was placed in aluminum pans and heated from 30 to 300 °C at 10 °C/min under a nitrogen purge of 50 mL/min. DSC was interpreted as evidence of thermal/solid-state changes and not, by itself, as proof of chemical compatibility.

Apparent Solubility Study

Apparent solubility was evaluated for pure ATC and the selected ATC-SNV formulation in acidic medium (0.1 N HCl, pH 1.2) and phosphate buffer (pH 6.8), with measurements performed in triplicate. Because equilibrium solubility is sensitive to equilibration and phase-separation conditions [12], the complete experimental procedure must be reported.

Apparent In Vitro Release Study

The apparent in vitro release/drug-transfer profiles of pure ATC dispersion and the selected ATC-SNV dispersion were evaluated using USP apparatus II coupled with a dialysis-bag diffusion method. Dialysis methods are widely used for nanoparticulate systems but measure a combination of drug release/solubilization and diffusion across the dialysis membrane [13,14]. A dialysis membrane with a molecular-weight cut-off (MWCO) of 14,000 Da was soaked in distilled water for 24 h before use.

An accurately measured volume of each dispersion containing an equivalent amount of ATC was placed separately in a pre-soaked dialysis bag. The bag was immersed in 900 mL phosphate buffer (pH 6.8) maintained at 37 ± 0.5 °C and stirred at 50 rpm.

At predetermined intervals, samples were withdrawn from the receptor medium and replaced immediately with an equal volume of fresh preheated medium. Samples were filtered and diluted as required and analyzed spectrophotometrically at the validated λmax. Experiments were performed in triplicate (n = 3), and results are reported as mean ± SD. Cumulative values should be corrected for drug removed during serial sampling if that correction was applied.

Ex Vivo Intestinal Permeation Study

Ex vivo intestinal permeation was evaluated using freshly excised jejunal segments from male albino rats. The manuscript reports approval by an Institutional Animal Ethics Committee (Approval No. EC131). Jejunal segments were rinsed with phosphate buffer (pH 6.8) to remove luminal contents and gently blotted before use.

One end of each jejunal segment was tied, the donor formulation was introduced into the lumen, and the other end was sealed. The intestinal sac was immersed in phosphate buffer (pH 6.8) maintained at 37 ± 0.5 °C under continuous stirring. The tissues were used immediately after isolation and kept moist with buffer, consistent with the general ex vivo intestinal-sac approach used in spanlastic studies [6].

At predetermined intervals, samples were withdrawn from the receptor medium and replaced with equal volumes of fresh preheated buffer. Samples were diluted as necessary and analyzed using the validated spectrophotometric method. Experiments were performed in triplicate (n = 3), and results are reported as mean ± SD. The manuscript reports flux, apparent permeability coefficient (Papp), and enhancement ratio (ER); the exact equations, linear time interval used for flux estimation, tissue area, donor concentration, and serial-sampling correction must be reported to make these calculations reproducible.

Statistical Analysis

Box-Behnken response models were evaluated by ANOVA at $p < 0.05$ using Design-Expert® Version 13. Replicate characterization data are presented as mean ± SD. Apparent release data were fitted to zero-order, first-order, Higuchi, Korsmeyer-Peppas, and Hixson-Crowell models. R^2 values were used descriptively for model fit, but mechanistic interpretation of the Korsmeyer-Peppas model additionally requires the release exponent (n), an appropriate fitting range, and residual/error assessment. For the ex vivo time-course data, the originally applied unpaired t-test is not an ideal analysis when repeated samples are obtained from the same experimental unit over time; a repeated-measures or mixed-effects approach would be preferable if the raw experimental structure permits reanalysis.

RESULTS AND DISCUSSION

Optimization and Evaluation of the Selected Formulation

The Box-Behnken design generated 15 experimental ATC-SNV formulations. Particle size, PDI, and EE% varied across the design space,

indicating formulation-dependent changes in vesicle properties. The design matrix and observed responses are presented in Table 3. The response data were analyzed by ANOVA and fitted to the most appropriate polynomial models supported by the available model statistics.

Effect of Formulation Variables on Particle Size

Particle size ranged from 59.63 to 404.1 nm across the experimental runs (Table 3). The smallest observed size (59.63 nm) occurred at a Span 60:Tween 80 ratio of 7:3, Soluplus 25 mg, and sonication time 10 min, whereas the largest observed size (404.1 nm) occurred at a ratio of 5:5, Soluplus 12.5 mg, and sonication time 10 min.

The relationship between the formulation variables and particle size was adequately described by a reduced quadratic model, as represented by the following coded equation:

$$PS\ (nm) = 371.97 - 56.86B - 100.99B^2 - 57.17C^2$$

ANOVA indicated that the reduced quadratic particle-size model was statistically significant ($F = 7.07$, $p = 0.0065$) with non-significant lack of fit ($F = 1.57$, $p = 0.4487$). However, predictive performance was modest ($R^2 = 0.6583$, adjusted $R^2 = 0.5652$, predicted $R^2 = 0.3775$; adequate precision = 7.0921). Accordingly, the model should be interpreted mainly within the studied design space and should not be described as strongly predictive. The predicted-versus-observed relationship is shown in Fig. 2.

The selected formulation showed an experimental particle size of 59.63 nm. This value is smaller than the optimized Soluplus-stabilized nimodipine spanlastic formulation reported by Alkufi and Kassab (125.7 ± 0.29 nm), although direct numerical comparison is limited by differences in drug, surfactant composition, design factors, and processing conditions [8].

Comparable nanoscale dimensions have been reported for other atorvastatin nanocarriers, although the carrier architectures differ. Li et al. obtained atorvastatin calcium-loaded PLGA nanoparticles with a mean diameter of 174.7 nm and approximately 71% encapsulation efficiency [15], whereas Shahraeini et al. reported atorvastatin solid lipid nanoparticles ranging from 71.07 to 202.07 nm with PDI values ≤0.5 [16]. These studies support the feasibility of producing atorvastatin-containing nanosystems in this size domain, but they do not establish direct superiority of the present spanlastic formulation.

Among the retained terms, Soluplus amount (B) and B^2 significantly influenced particle size ($p < 0.05$), whereas C^2 was not statistically significant ($p > 0.05$). As shown in Fig. 3, the fitted response

Table 3. Box-Behnken experimental design and observed responses for ATC-SNV formulations.

Run	Soluplus (mg)	ST (min)	Span 60:Tween 80	PS (nm)	PDI	EE (%)
1	12.5	0	9:1	261.7	0.538	95
2	12.5	10	9:1	278.8	0.468	92.6
3	12.5	0	5:5	374.4	0.685	77.8
4	12.5	10	5:5	404.1	0.727	72.2
5	0	5	9:1	309.3	0.528	94.2
6	25	5	9:1	233.5	0.432	93.5
7	0	5	5:5	322.6	0.437	75
8	25	5	5:5	278.3	0.543	72.64
9	0	0	7:3	310.6	0.471	90.86
10	25	0	7:3	170.7	0.39	90.2
11	0	10	7:3	254.5	0.505	85.5
12	25	10	7:3	59.63	0.277	84
13 (C1)	12.5	5	7:3	375.4	0.606	87.3
14 (C2)	12.5	5	7:3	384.4	0.444	86.4
15 (C3)	12.5	5	7:3	296.3	0.539	88.2

ST, sonication time; PS, particle size; PDI, polydispersity index; EE, entrapment efficiency; C1-C3, center-point replicates.

varied nonlinearly with Soluplus amount. The negative linear coefficient for B is consistent with a general reduction in particle size as Soluplus increased over the studied range, although the significant quadratic term indicates that this relationship should not be interpreted as strictly linear. Steric stabilization and reduced aggregation are plausible explanations for the observed effect of Soluplus [7,8].

A Soluplus/Pluronic F127 micellar system for lapatinib formed nanocolloids of 92.9 ± 4.07 nm with approximately 87% drug encapsulation [17]. Although that study used a different drug and carrier architecture, it provides independent evidence that Soluplus can participate in nanoscale colloidal assemblies; therefore, the particle-size effect observed here is mechanistically plausible but remains formulation-specific.

Effect of Independent Variables on Polydispersity Index (PDI)

The PDI values ranged from 0.277 to 0.727 across the Box-Behnken runs (Table 3), demonstrating substantial variation in particle-size distribution among formulations. Lower PDI values represent narrower distributions, but interpretation should consider the measurement method and the overall formulation context.

ANOVA showed that the reduced quadratic model for PDI was not statistically significant ($p > 0.05$). Accordingly, no statistically supported mechanistic conclusion regarding the effects of the investigated factors on PDI can be drawn from this model, and PDI was not used as a modeled response in numerical optimization. The observed PDI values are therefore reported descriptively.

The lowest observed PDI (0.277) occurred for the formulation containing Soluplus 25 mg, 10 min sonication, and a Span 60:Tween 80 ratio of 7:3, whereas the highest PDI (0.727) occurred at Soluplus 12.5 mg, 10 min sonication, and a 5:5 ratio. Only one experimental run had PDI < 0.30; therefore, the dataset should not be described as containing several formulations below this threshold.

From an optimization perspective, the selected

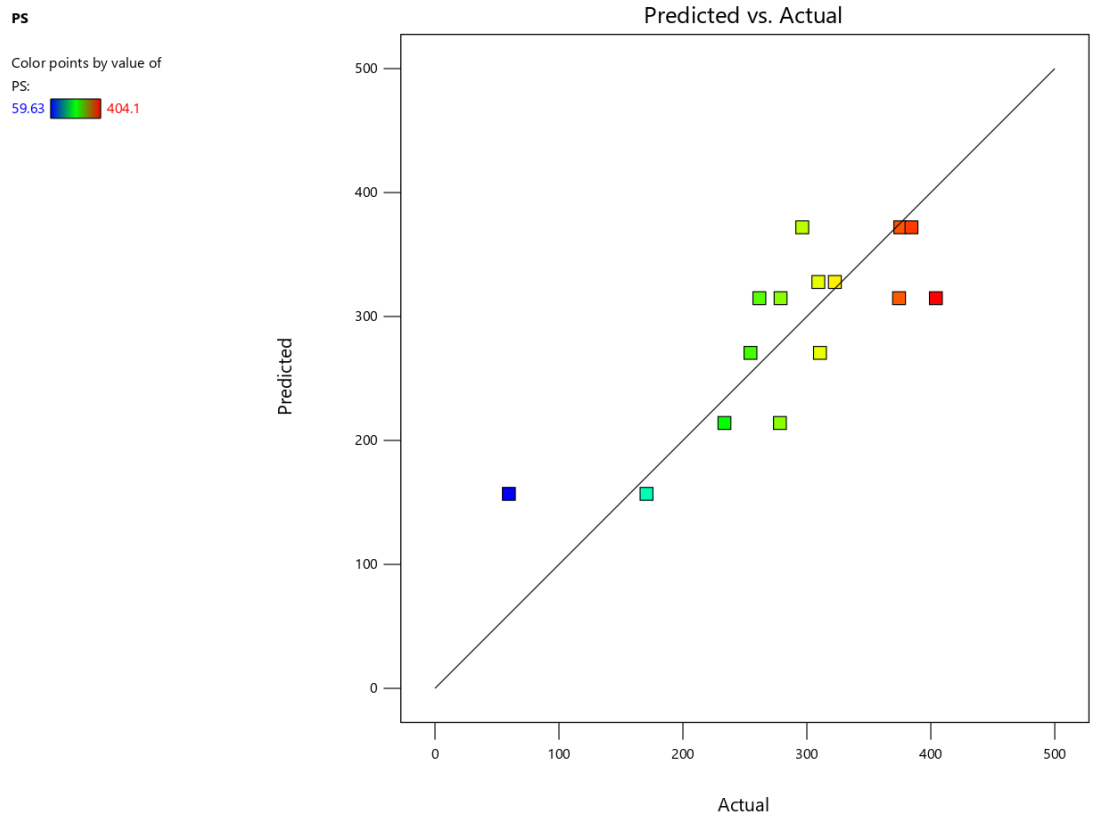

Fig. 2. Predicted versus actual particle-size values obtained from the reduced quadratic model for ATC-SNVs.

run's PDI of 0.277 is favorable, but it should be treated as an observed property rather than a statistically optimized response because the PDI model was non-significant. The broad PDI values in several other runs (up to 0.727) also indicate that size-distribution control was not robust across the full design space. Independent replicate batches are therefore needed to establish reproducibility of the selected PDI.

Effect of Independent Variables on Entrapment Efficiency (EE%)

Entrapment efficiency ranged from 72.2% to 95.0% across the experimental runs (Table 3), indicating substantial ATC entrapment under all tested conditions while also demonstrating a clear formulation effect.

The relationship between the formulation variables and EE% was adequately described by a quadratic model, as represented by the following coded equation:

$$EE\ (\%) = 87.30 + 9.71A - 0.6525B - 2.45C + 0.4150AB + 0.8000AC - 0.2100BC - 3.35A^2 - 0.1125B^2 + 0.4525C^2$$

ANOVA showed that the quadratic EE% model was significant ($F = 116.52$, $p < 0.0001$) with non-significant lack of fit ($F = 1.00$, $p = 0.5339$). The model showed excellent fit statistics within the design space ($R^2 = 0.9953$, adjusted $R^2 = 0.9867$, predicted $R^2 = 0.9501$, adequate precision = 33.0264). The close agreement between predicted and observed EE% values is illustrated in Fig. 4.

The selected formulation had an experimental EE of 84.0%. Alkufi and Kassab reported EE of 85.43 ± 0.17% for their optimized Soluplus-stabilized nimodipine spanlastic formulation [8]. The similarity is descriptive only because the incorporated drugs, surfactant systems, experimental designs, and preparation conditions differed between studies.

Among the investigated factors, the Span

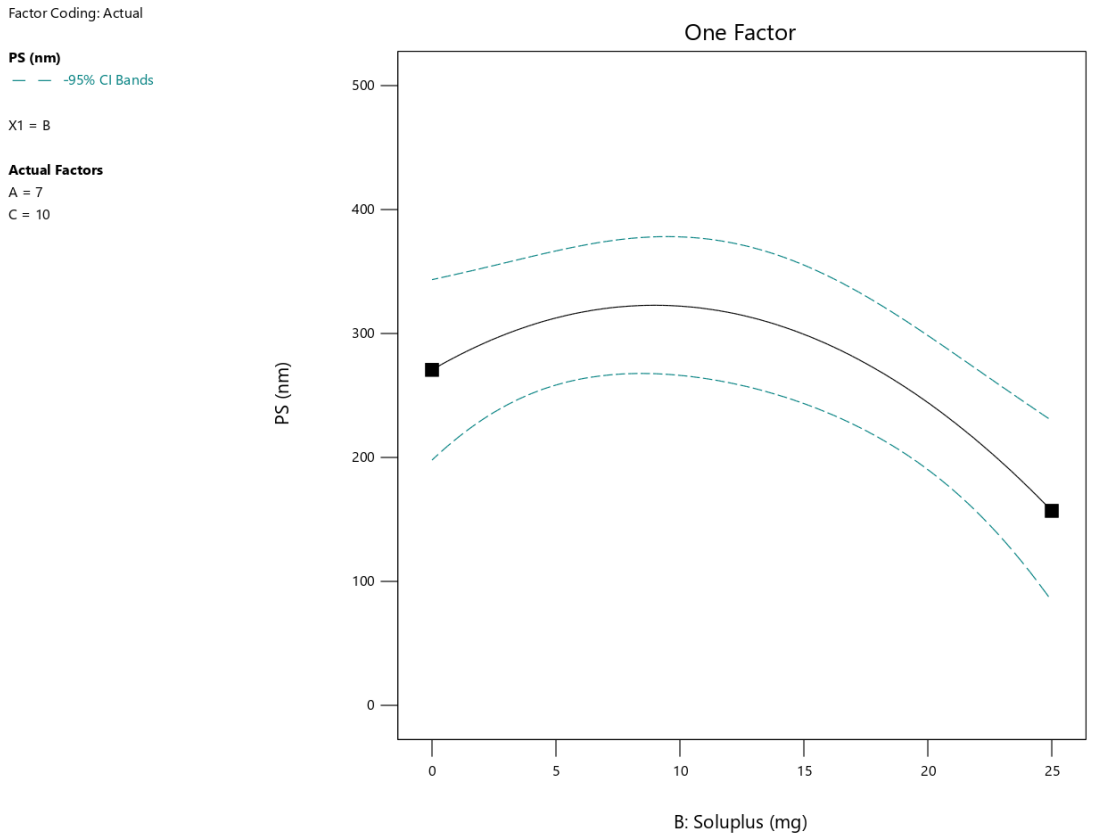

Fig. 3. One-factor plot showing the modeled effect of Soluplus amount (B) on particle size of ATC-SNVs within the studied design space.

60:Tween 80 ratio (A) exerted the largest modeled effect on EE%, as indicated by its F-value, followed by sonication time (C) and A^2. Importantly, the coding of factor A is 5:5 = -1, 7:3 = 0, and 9:1 = +1; therefore, the positive A coefficient is consistent with higher EE% as the Span 60 proportion increased. Longer sonication showed a negative linear effect on EE%, which may reflect greater drug leakage or vesicle disruption. The response-surface plots in Fig. 5A and Fig. 5B show the combined effects of surfactant ratio and Soluplus amount at 10 min sonication.

Similar sensitivity of vesicular entrapment to surfactant composition has been observed in related nanocarrier systems. In Span 60-based nanospanlastics containing Tween 80 or Cremophor RH 40, Badria et al. reported an optimized EE of 90.32 ± 2.18% [18]. In atorvastatin solid lipid nanoparticles, surfactant hydrophilic-lipophilic balance also influenced particle size, zeta potential, and entrapment efficiency [16]. These comparisons support a qualitative role for surfactant composition, while differences in drug, route, carrier architecture, and processing preclude direct numerical equivalence.

The highest observed EE% (95.0%) occurred at Soluplus 12.5 mg, no sonication, and a Span 60:Tween 80 ratio of 9:1, while the lowest value (72.2%) occurred at Soluplus 12.5 mg, 10 min sonication, and a 5:5 ratio. For the selected run, experimental EE (84.0%) was close to the model-predicted value (approximately 83.6%), supporting the EE model at that design point. This agreement should not be generalized to particle-size validation, for which the prediction error was much larger.

The selected formulation should therefore be described as a multi-response compromise rather than as the formulation that maximized EE% alone, because the highest experimental EE% (95.0%) occurred under different factor settings. This distinction is important when interpreting the desirability-based selection.

Numerical Optimization and Selection of the Formulation

Numerical optimization used a desirability-function approach to minimize particle size

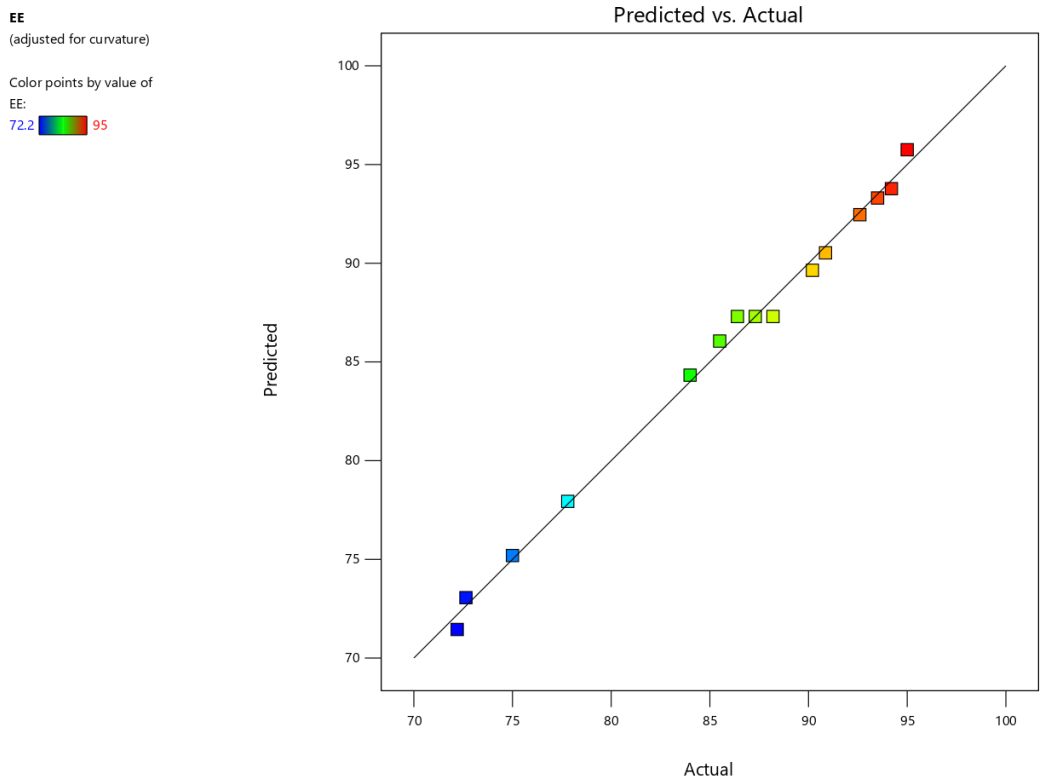

Fig. 4. Predicted versus actual entrapment-efficiency (EE%) values obtained from the quadratic model.

and maximize EE%. Because the PDI model was statistically non-significant, PDI was excluded from the numerical optimization. The selected formulation corresponded to a Span 60:Tween 80 ratio of 7:3, Soluplus 25 mg, and sonication time 10 min, with an overall desirability of 0.835. The numerical optimization and desirability ramp are shown in Fig. 6.

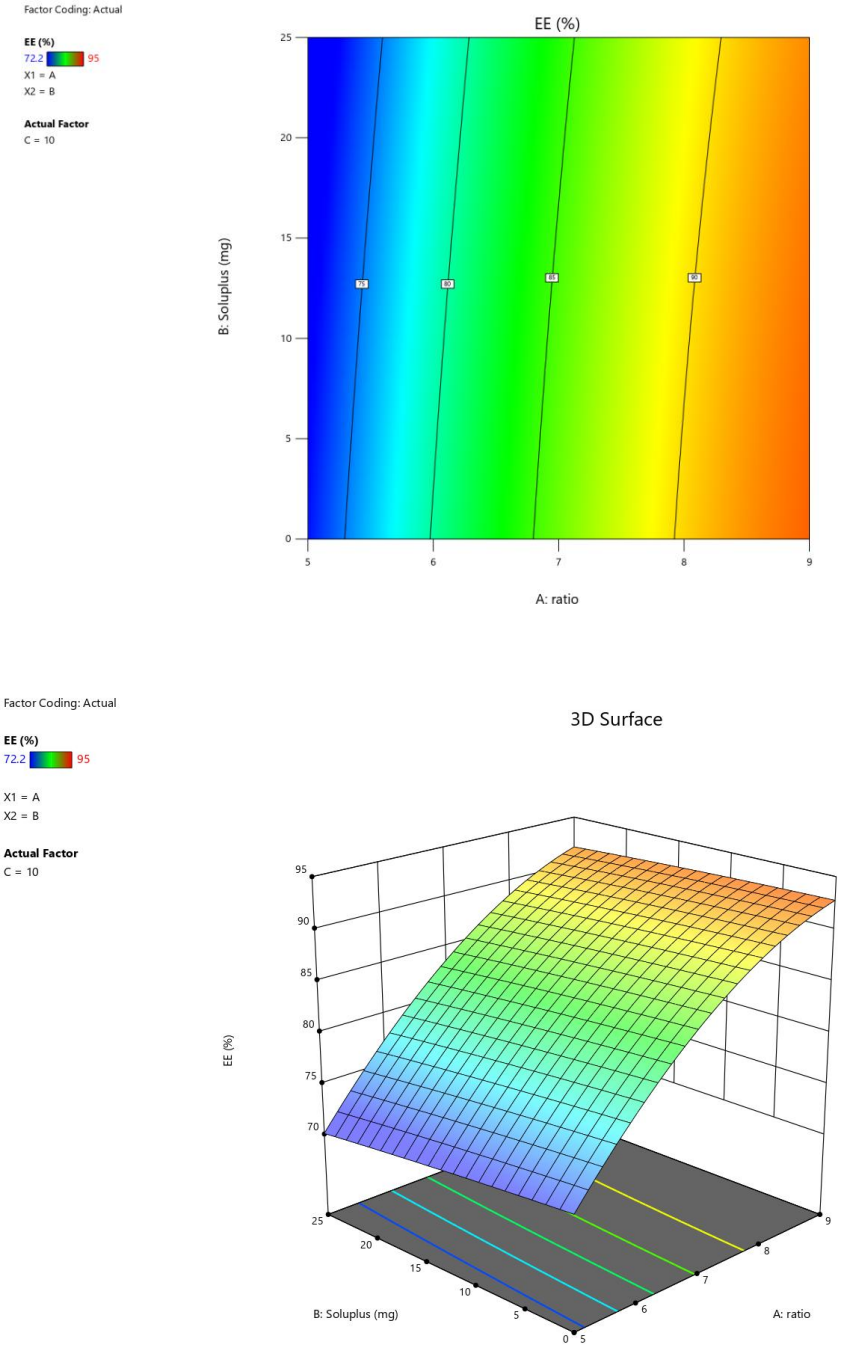

Fig. 5. A) Contour plot of the modeled effects of Span 60:Tween 80 ratio (A) and Soluplus amount (B) on EE% at 10 min sonication. B) Three-dimensional response-surface plot of the modeled effects of Span 60:Tween 80 ratio (A) and Soluplus amount (B) on EE% at 10 min sonication.

For the selected design run, the predicted particle size was approximately 156.95 nm whereas the experimentally observed value was 59.63 nm, indicating substantial prediction error for this response. In contrast, predicted and experimental EE values were closely aligned (approximately 84%). Because the selected composition was already one of the experimental design runs, these observations do not constitute independent external validation. A separately prepared confirmation batch at a model-predicted optimum would be required for stronger validation of the optimization.

Characterization of the Selected ATC-SNV Formulation

The selected formulation was characterized to assess surface charge, vesicle deformability, morphology, thermal behavior, apparent solubility, apparent in vitro release, and ex vivo intestinal permeation.

Zeta Potential

The zeta-potential distribution is shown in Fig. 7. The selected ATC-SNV formulation exhibited a zeta potential of -43.1 mV. The relatively high magnitude of the negative surface potential is consistent with an electrostatic contribution to colloidal stabilization under the measurement conditions, while Soluplus and non-ionic surfactants may also provide steric stabilization [7,8]. Zeta potential alone, however, does not demonstrate long-term physical stability; dedicated storage-stability studies are required.

Negative zeta potentials have also been reported for atorvastatin nanoparticles prepared with non-ionic Tween/Span surfactants [16], showing that a negative electrokinetic potential can arise from the complete interfacial composition even when the principal surfactants are non-ionic. Nevertheless, zeta potential is strongly medium-dependent and cannot substitute for time-resolved physical-stability testing.

Vesicle Deformability

In the deformability experiment, particle size decreased from 201.1 nm before extrusion to 187.9 nm after extrusion, and the reported DI was 10.21. These particle sizes were obtained under a different experimental workflow from the optimization-stage DLS measurement (59.63 nm) and therefore should not be treated as directly interchangeable. The result is consistent with vesicle deformability, but the absolute DI cannot be independently evaluated until the extrusion

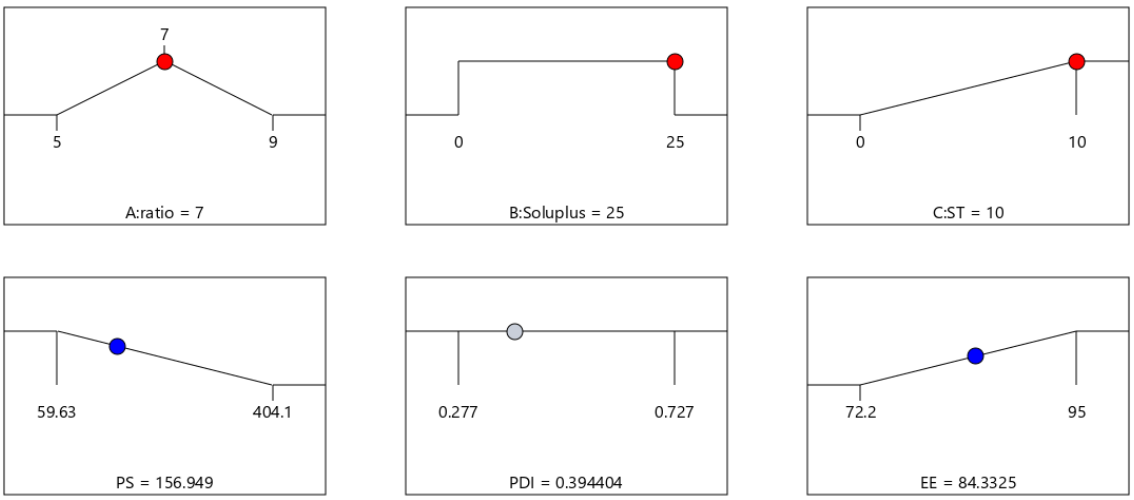

Fig. 6. Ramp plot and desirability function used for numerical selection of the ATC-SNV formulation.

time/flux term J and its units are fully reported.

Tween 80 functions as an edge activator and can increase bilayer flexibility; this provides a plausible basis for the ability of spanlastic vesicles to deform under extrusion [5,11]. Nevertheless, the present data support deformability under the reported test conditions and should not, by themselves, be used to quantify intestinal transport mechanisms.

Badria et al. also characterized Span 60/edge-activator nanospanlastics as deformable vesicles

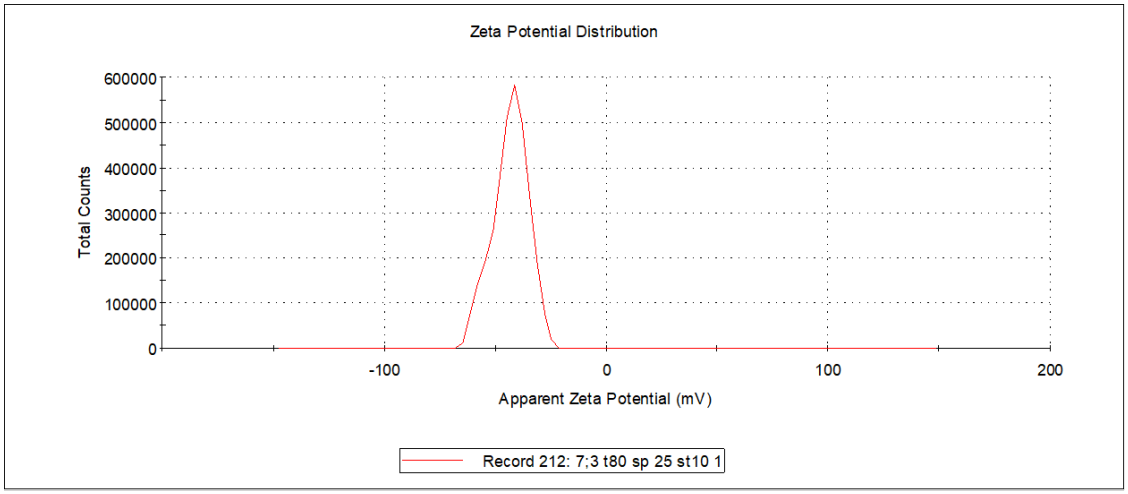

Fig. 7. Zeta-potential distribution of the selected ATC-SNV formulation.

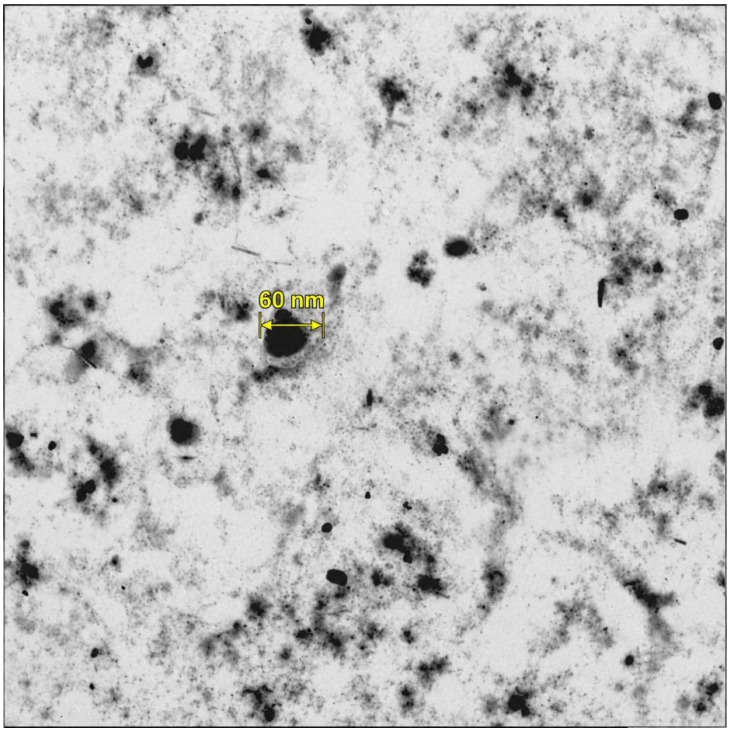

Fig. 8. TEM image of the selected ATC-SNV formulation showing nanoscale vesicular structures; the displayed measurement is approximately 60 nm.

and observed enhanced ex vivo permeation in a different delivery setting [18]. This supports the general contribution of edge activators to vesicle deformability, but it does not establish that the numerical DI reported here directly predicts intestinal permeation.

Transmission Electron Microscopy (TEM)

TEM imaging (Fig. 8) showed predominantly rounded nanoscale structures, with an example particle dimension of approximately 60 nm. This observation is in the same nanoscale range as the selected formulation's DLS result; however, TEM and DLS measure different particle characteristics (dry/stained projected dimensions versus hydrodynamic diameter), so exact numerical equivalence should not be expected.

Scanning Electron Microscopy (SEM)

Fig. 9 shows the SEM micrograph of the lyophilized selected ATC-SNV formulation. The dried sample exhibited an aggregated, porous morphology rather than clearly separated individual vesicles. Aggregation can occur during drying/lyophilization; therefore, SEM is best interpreted here as characterization of the dried powder surface, whereas vesicle-scale morphology is more appropriately assessed by TEM.

Differential Scanning Calorimetry (DSC)

DSC thermograms of pure ATC, the physical mixture, and the selected ATC-SNV formulation are presented in Fig. 10. Pure ATC showed a sharp endothermic transition at 158.28 °C, consistent with a crystalline melting event under the test conditions.

The physical mixture showed multiple thermal transitions, including an endothermic event at approximately 147.74 °C. The shift and reduced prominence of the ATC-related transition may reflect physical mixing and altered crystalline organization in the presence of formulation components. The absence of an obvious new DSC peak is not sufficient evidence to exclude chemical incompatibility.

The selected ATC-SNV formulation showed a prominent endothermic transition at approximately 51.93 °C, while the characteristic ATC melting peak was not evident. This finding is consistent with a marked reduction in detectable

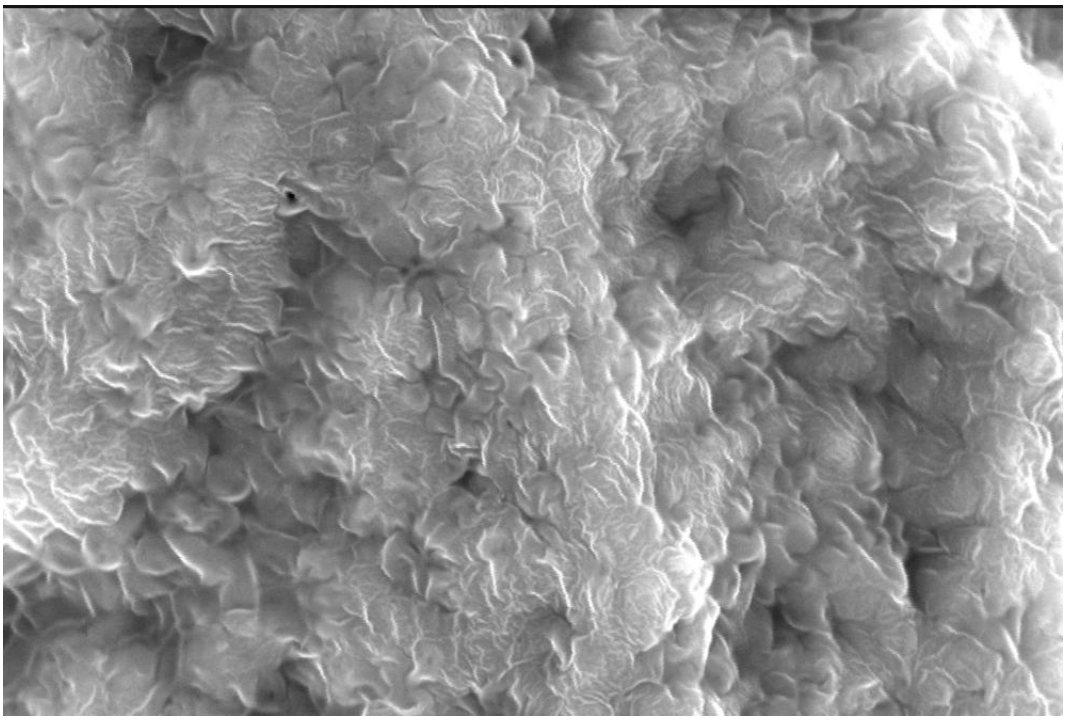

Fig. 9. SEM micrograph of the lyophilized selected ATC-SNV formulation.

ATC crystallinity and/or molecular dispersion within the formulation matrix. It should not be described as definitive proof of molecular incorporation or chemical compatibility without complementary solid-state techniques such as powder X-ray diffraction and appropriate spectroscopic analysis.

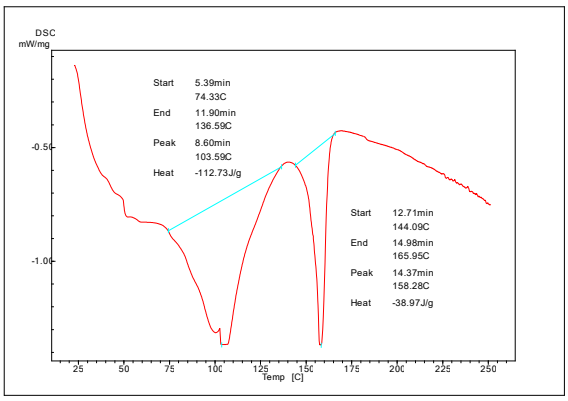

A. Pure atorvastatin calcium (ATC).

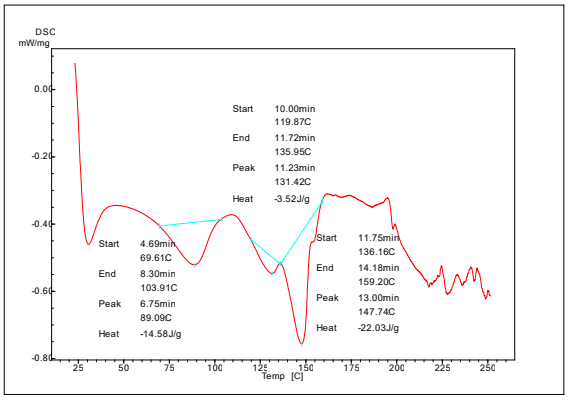

B. Physical mixture (PM).

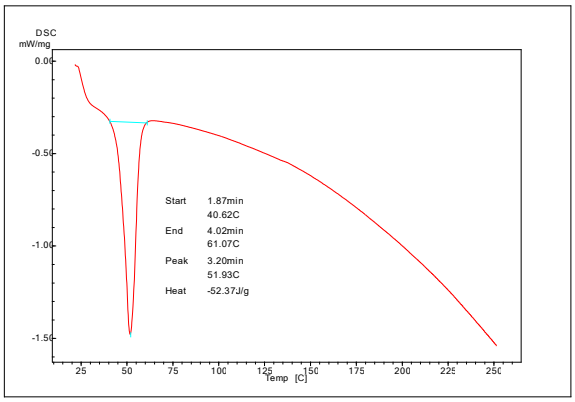

C. Selected ATC-SNV formulation.

Fig. 10. DSC thermograms shown as (A) pure ATC, (B) physical mixture (PM), and (C) selected ATC-SNV formulation.

Notably, the 51.93 °C transition lies close to the thermal transition reported for Span 60-containing niosomal matrices (around 55 °C) [19]. Accordingly, this endotherm may predominantly reflect the surfactant-rich vesicular matrix and should not be assigned specifically to ATC incorporation. In atorvastatin formulations, Dong et al. interpreted solid-state changes using DSC together with PXRD and FTIR [20], while Zidan et al. used FTIR and PXRD to demonstrate atorvastatin complexation and amorphous character in cyclodextrin-based nanosponges [21]. These studies reinforce that complementary solid-state analysis is required for a stronger conclusion.

Apparent Solubility Study

Pure ATC showed apparent solubility values of 15.55 ± 1.8 µg/mL at pH 1.2 and 241.8 ± 2.5 µg/mL at pH 6.8 (Table 4), demonstrating pronounced pH-dependent solubility under the tested conditions. These two measurements alone should not be used to assign a BCS category because formal BCS solubility classification also depends on dose-related solubility criteria and permeability [2]. The selected ATC-SNV formulation showed higher apparent solubility values of 343.5 ± 3.2 and 443.8 ± 4.1 µg/mL in the corresponding media.

The higher apparent solubility of the selected formulation is consistent with the combined effects of nanoscale dispersion, surfactant-mediated wetting/solubilization, Soluplus, and reduced detectable crystallinity. Because the exact equilibration and phase-separation procedure is not fully reported in the current Methods, the results are conservatively described as apparent solubility until the experimental protocol is

Table 4. Apparent solubility of pure ATC and the selected ATC-SNV formulation in the tested media.

Medium	Pure ATC (µg/mL)	Selected ATC-SNVs (µg/mL)
pH 1.2	15.55 ± 1.8	343.5 ± 3.2
pH 6.8	241.8 ± 2.5	443.8 ± 4.1

Data are presented as mean ± SD (n = 3).

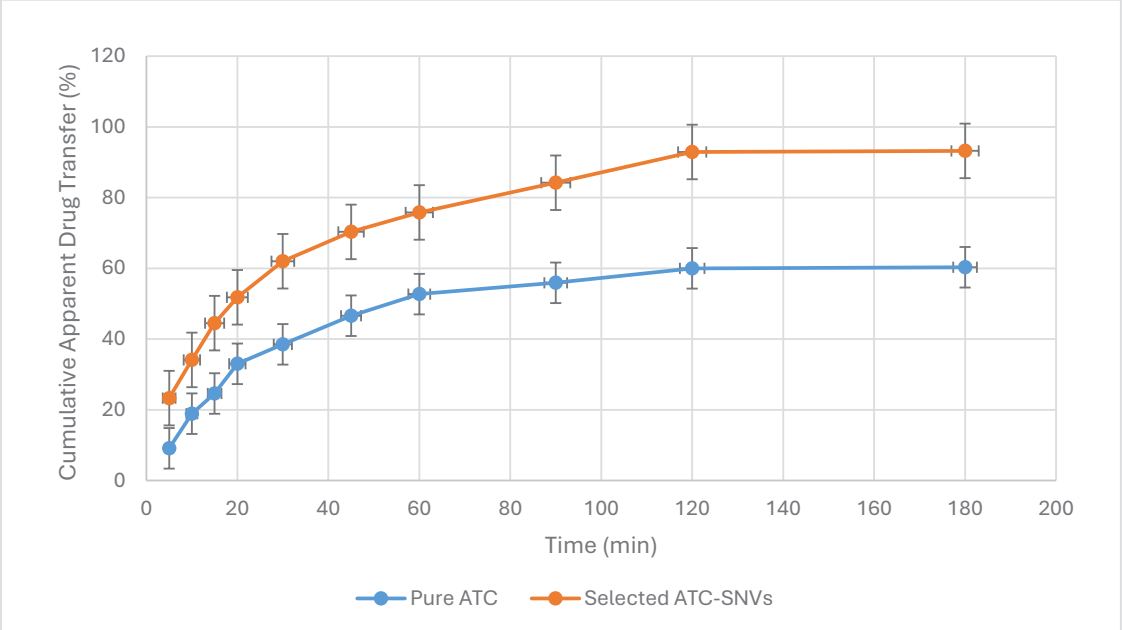

Fig. 11. Apparent in vitro drug-transfer profiles of pure ATC dispersion and the selected ATC-SNV formulation in phosphate buffer (pH 6.8) using the dialysis-bag method. Data are mean ± SD (n = 3).

completed [12].

Quantitatively, the apparent solubility increased by approximately 22.1-fold at pH 1.2 (343.5/15.55) and 1.84-fold at pH 6.8 (443.8/241.8) relative to pure ATC. The marked difference between these fold changes indicates that the formulation benefit is medium-dependent and should not be summarized using a single solubility-enhancement factor. Improved atorvastatin solubility has also been reported with Poloxamer 188 solid dispersions [20] and with pentaerythritol-Eudragit RS100 solid dispersions, the latter showing an approximately 43-fold increase in water solubility [22]. Because the dosage forms and analytical conditions differ, only the direction of effect—not the absolute magnitude—should be compared.

Apparent In Vitro Release Study

The dialysis-based profiles of pure ATC dispersion and the selected ATC-SNV formulation are presented in Fig. 11 as mean ± SD (n = 3). At 5 min, the measured cumulative drug transfer was 23.3 ± 1.4% for ATC-SNVs compared with 9.1 ± 0.8% for pure ATC. The selected formulation reached 92.9 ± 3.1% at 120 min and 93.2 ± 3.0% at 180 min, whereas pure ATC reached 60.3 ± 2.6% at 180 min.

The selected formulation therefore showed a rapid initial phase followed by a slower approach to a plateau. The very small increase between 120 and 180 min indicates that most measurable drug transfer had occurred by 120 min; the profile should not be described as evidence of prolonged sustained release beyond the experimental period.

The higher apparent drug transfer may be associated with improved wetting/solubilization, the nanoscale formulation, Soluplus and Tween 80, and reduced detectable ATC crystallinity. However, the dialysis method introduces a second transport barrier: drug must first become available outside the vesicles and then diffuse across the membrane. Consequently, the observed profile represents apparent release/drug transfer rather than direct intrinsic release from individual vesicles [13,14].

The apparent release data were fitted to zero-order, first-order, Higuchi, Korsmeyer-Peppas, and Hixson-Crowell models (Table 5). Korsmeyer-Peppas gave the highest reported R^2 (0.9477), followed by first-order (0.9112). The negative R^2 for the zero-order fit (-0.2527) indicates very poor fit relative to a simple mean-based baseline. A mechanistic release conclusion should not be assigned from R^2 alone.

For the Korsmeyer-Peppas model, the release exponent (n), the fraction of the profile used for fitting, and residual/error diagnostics should be reported before a transport mechanism is assigned. In addition, because the profile was generated with a dialysis membrane, kinetic parameters describe the overall apparent transfer process and may be influenced by membrane diffusion [14].

Improved atorvastatin dissolution has also been demonstrated in Poloxamer 188 solid dispersions [20] and cyclodextrin-based nanosponges [21], with the latter exhibiting a biphasic release pattern. The present findings are directionally consistent with those reports; however, the dialysis membrane in the current experiment adds a transport barrier, so the fitted kinetic models describe a composite apparent transfer process rather than intrinsic release from the vesicles alone.

Ex Vivo Intestinal Permeation Study

The ex vivo intestinal permeation profiles of pure ATC dispersion and the selected ATC-SNV formulation across rat jejunal tissue are shown in Fig. 12 as mean ± SD (n = 3). Pure ATC increased from 2.55 ± 0.50% at 5 min to 54.31 ± 2.20% at 240 min, whereas the selected ATC-SNV formulation increased from 23.84 ± 1.30% to 96.30 ± 2.80% over the same interval.

Table 5. Kinetic-model fitting of the apparent in vitro release/drug-transfer profile of the selected ATC-SNV formulation.

Model	R^2
Zero-order	-0.2527
First-order	0.9112
Higuchi	0.7532
Korsmeyer–Peppas	0.9477
Hixson–Crowell	0.7836

Reported flux values were 2.69 µg/cm²/min for pure ATC and 5.40 µg/cm²/min for the selected ATC-SNVs, with reported Papp values of 4.49×10^{-5} and 9.00×10^{-5} cm/s, respectively. The corresponding enhancement ratio was approximately 2 (Table 6). These ex vivo findings support improved permeation under the test conditions but do not establish increased systemic exposure or oral bioavailability.

The improved ex vivo permeation is plausibly related to the higher apparent solubility and drug availability of ATC in the selected formulation, together with the effects of Tween 80, Soluplus, nanoscale dispersion, and vesicle deformability. Similar enhancement of intestinal permeation has been reported for EGCG-loaded nanospanlastics, although direct quantitative comparison is limited by differences in drug, formulation, tissue preparation, and experimental conditions [6].

At 240 min, the cumulative permeated fraction was approximately 1.77-fold higher for the selected ATC-SNVs than for pure ATC (96.30% vs 54.31%), whereas the reported flux and Papp were each approximately 2.0-fold higher. These are related but distinct endpoints and should not be conflated. Telange et al. similarly reported enhanced ex vivo permeation of atorvastatin from a solid-dispersion system together with increased solubility and dissolution [22], supporting the general relationship between improved drug availability and ex vivo transport while not establishing the specific transport mechanism of the present spanlastic system.

Limitations

This study has several important limitations. First,

Table 6. Reported ex vivo permeation parameters of pure ATC dispersion and the selected ATC-SNV formulation across rat jejunal tissue.

Formulation	Flux (µg/cm²/min)	Papp (cm/s)	ER
Pure ATC dispersion	2.69	4.49×10^{-5}	1
Selected ATC-SNVs	5.4	9.00×10^{-5}	2

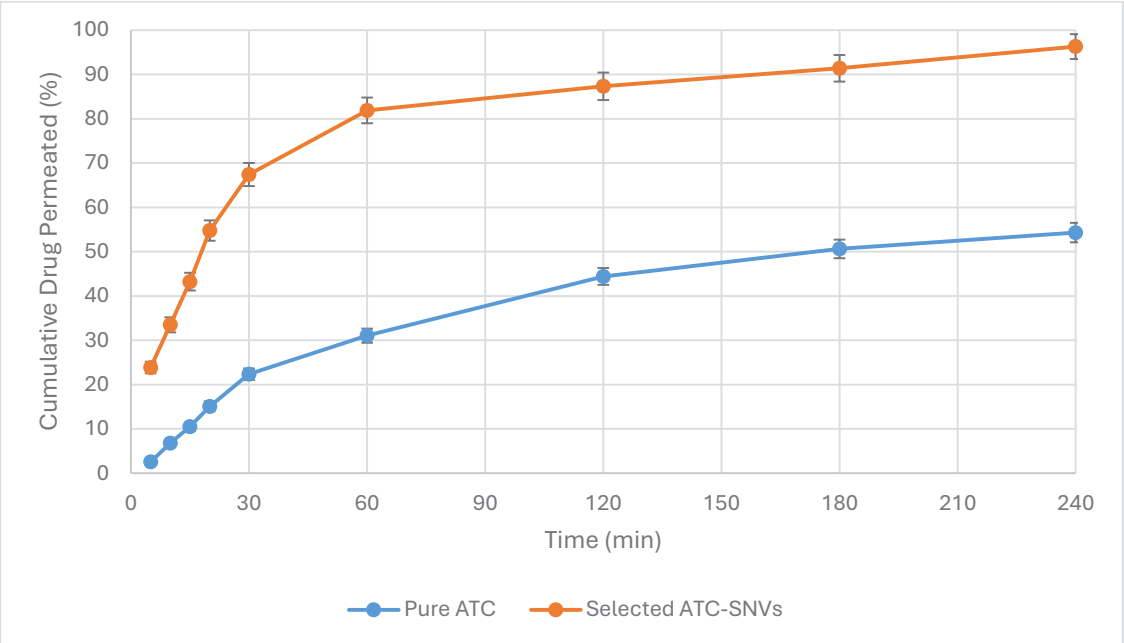

Fig. 12. Ex vivo intestinal permeation profiles of pure ATC dispersion and the selected ATC-SNV formulation across rat jejunal tissue. Data are mean ± SD (n = 3).

no in vivo pharmacokinetic or pharmacodynamic experiment was performed; therefore, the present data cannot demonstrate improved oral bioavailability or therapeutic efficacy. Second, long-term physical and chemical stability was not evaluated. Third, the particle-size model had modest predictive performance, and the selected formulation was an existing design run rather than an independently prepared confirmation point. Fourth, the ex vivo experiment used only three replicates, and the repeated time-course structure requires a statistical approach appropriate to repeated measurements when the same tissue sacs are sampled longitudinally. Fifth, the dialysis-bag study reflects combined formulation release/solubilization and membrane diffusion and therefore represents apparent drug transfer rather than intrinsic vesicle release. Sixth, DSC alone cannot establish chemical compatibility or fully define ATC solid state. Finally, several essential reproducibility details remain to be supplied by the authors, including complete formulation volumes/process settings, ultrafiltration relative centrifugal force, DI extrusion time/flux, complete apparent-solubility procedure, analytical calibration details, and full animal/tissue/permeation calculation information. Future work should include an independent confirmation batch, long-term stability, complementary solid-state characterization, statistically appropriate analysis of repeated ex vivo measurements, and in vivo pharmacokinetic evaluation.

CONCLUSION

Soluplus-stabilized atorvastatin calcium-loaded spanlastic nanovesicles were prepared by ethanol injection and evaluated using a Box-Behnken formulation design. The selected formulation showed nanoscale particle size, PDI of 0.277, EE of 84.0%, a zeta potential of -43.1 mV, and measurable deformability. Compared with pure ATC dispersion, it showed higher apparent solubility, greater apparent drug transfer in the dialysis-based in vitro study, and approximately two-fold higher reported ex vivo flux and Papp. These findings demonstrate improved pharmaceutical and ex vivo transport performance under the investigated conditions. Nevertheless, the limited predictive accuracy of the particle-size model, absence of independent confirmation and long-term stability testing, incomplete reporting of several experimental details, and lack of in vivo pharmacokinetic data preclude conclusions about clinical performance or improved oral bioavailability. Additional confirmation, stability, solid-state, and in vivo studies are required before translational claims can be made.

CONFLICT OF INTEREST

The authors declare that there is no conflict of interests regarding the publication of this manuscript.

REFERENCES

1. Xie B, Liu Y, Li X, Yang P, He W. Solubilization techniques used for poorly water-soluble drugs. Acta Pharmaceutica Sinica B. 2024;14(11):4683-4716.
2. Amidon GL, Lennernäs H, Shah VP, Crison JR. A Theoretical Basis for a Biopharmaceutic Drug Classification: The Correlation of in Vitro Drug Product Dissolution and in Vivo Bioavailability. Pharm Res. 1995;12(3):413-420.
3. Dressman JB, Reppas C. In vitro–in vivo correlations for lipophilic, poorly water-soluble drugs. Eur J Pharm Sci. 2000;11:S73-S80.
4. Pınar SG, Oktay AN, Karaküçük AE, Çelebi N. Formulation Strategies of Nanosuspensions for Various Administration Routes. Pharmaceutics. 2023;15(5):1520.
5. Kakkar S, Kaur IP. Spanlastics—A novel nanovesicular carrier system for ocular delivery. Int J Pharm. 2011;413(1-2):202-210.
6. Mazyed EA, Helal DA, Elkhoudary MM, Abd Elhameed AG, Yasser M. Formulation and Optimization of Nanospanlastics for Improving the Bioavailability of Green Tea Epigallocatechin Gallate. Pharmaceuticals. 2021;14(1):68.
7. Guembe-Michel N, Nguewa P, González-Gaitano G. Soluplus®-Based Pharmaceutical Formulations: Recent Advances in Drug Delivery and Biomedical Applications. Int J Mol Sci. 2025;26(4):1499.
8. Alkufi HK, Kassab HJ. Soluplus-Stabilized Nimodipine-Entrapped Spanlastic Formulations Prepared with Edge Activator (Tween20): Comparative Physicochemical Evaluation. Pharmaceutical Nanotechnology. 2025;13(3):551-563.
9. Corsini A, Bellosta S, Baetta R, Fumagalli R, Paoletti R, Bernini F. New insights into the pharmacodynamic and pharmacokinetic properties of statins. Pharmacology and Therapeutics. 1999;84(3):413-428.
10. МЕДИЧНЕ ЦИТУВАННЯ: ПУТІВНИК NLM ДЛЯ АВТОРІВ, РЕДАКТОРІВ І ВИДАВЦІВ. Morphologia. 2021;15(2):77-82.
11. El Zaafarany GM, Awad GAS, Holayel SM, Mortada ND. Role of edge activators and surface charge in developing ultradeformable vesicles with enhanced skin delivery. Int J Pharm. 2010;397(1-2):164-172.
12. Baka E, Comer JEA, Takács-Novák K. Study of equilibrium solubility measurement by saturation shake-flask method using hydrochlorothiazide as model compound. Journal of Pharmaceutical and Biomedical Analysis. 2008;46(2):335-341.
13. Shen J, Burgess DJ. In vitro dissolution testing strategies for nanoparticulate drug delivery systems: recent developments and challenges. Drug Delivery and Translational Research. 2013;3(5):409-415.

14. Modi S, Anderson BD. Determination of Drug Release Kinetics from Nanoparticles: Overcoming Pitfalls of the Dynamic Dialysis Method. Mol Pharm. 2013;10(8):3076-3089.
15. Li Z, Tao W, Zhang D, Wu C, Song B, Wang S, et al. The studies of PLGA nanoparticles loading atorvastatin calcium for oral administration in vitro and in vivo. Asian Journal of Pharmaceutical Sciences. 2017;12(3):285-291.
16. Shahraeini SS, Akbari J, Saeedi M, Morteza-Semnani K, Abootorabi S, Dehghanpoor M, et al. Atorvastatin Solid Lipid Nanoparticles as a Promising Approach for Dermal Delivery and an Anti-inflammatory Agent. AAPS PharmSciTech. 2020;21(7).
17. Bonde GV, Ajmal G, Yadav SK, Mittal P, Singh J, Bakde BV, et al. Assessing the viability of Soluplus® self-assembled nanocolloids for sustained delivery of highly hydrophobic lapatinib (anticancer agent): Optimisation and in-vitro characterisation. Colloids Surf B Biointerfaces. 2020;185:110611.
18. Badria FA, Fayed HA, Ibraheem AK, State AF, Mazyed EA. Formulation of Sodium Valproate Nanospanlastics as a Promising Approach for Drug Repurposing in the Treatment of Androgenic Alopecia. Pharmaceutics. 2020;12(9):866.
19. Mazzotta E, Romeo M, Hafidi Z, Perez L, Perrotta ID, Muzzalupo R. Design of Thermosensitive Niosomes by Eutectic Mixture of Natural Fatty Acids. Pharmaceutics. 2024;16(7):909.
20. Dong W, Su X, Xu M, Hu M, Sun Y, Zhang P. Preparation, characterization, and in vitro/vivo evaluation of polymer-assisting formulation of atorvastatin calcium based on solid dispersion technique. Asian Journal of Pharmaceutical Sciences. 2018;13(6):546-554.
21. Zidan MF, Ibrahim HM, Afouna MI, Ibrahim EA. In vitro and in vivo evaluation of cyclodextrin-based nanosponges for enhancing oral bioavailability of atorvastatin calcium. Drug Development and Industrial Pharmacy. 2018;44(8):1243-1253.
22. Telange DR, Bhaktani NM, Hemke AT, Pethe AM, Agrawal SS, Rarokar NR, et al. Development and Characterization of Pentaerythritol-EudragitRS100 Co-processed Excipients as Solid Dispersion Carriers for Enhanced Aqueous Solubility, In Vitro Dissolution, and Ex Vivo Permeation of Atorvastatin. ACS Omega. 2023;8(28):25195-25208.